City, University of London Institutional Repository

This is the accepted version of the paper.

This version of the publication may differ from the final published version.

Rotor Profile Design and Numerical Analysis of 2-3 type

Multiphase Twin-screw Pumps

Di Yan[1, 2], Qian Tang[1*], Ahmed Kovacevic[2], Sham Rane[2]

[1] State Key Laboratory of Mechanical Transmission, Chongqing University, 400044, China;

[2]Centre for Compressor Technology, City University London, EC1V0HB, UK;

Abstract: Increasing demands for high-performance handling of fluids in oil and gas as well as other applications require improvements of efficiency and reliability of screw pumps. Rotor profile plays the key role in the performance of such machines. This paper analyses difference in performance of 2-3 lobe combination of a twin screw pumps with different rotor profiles. A-type profile formed of involute-cycloid curves and D-type formed of cycloid curves are typical representatives for 2-3 type screw pumps. The investigation is performed by use of a full 3-D Computational Fluid Dynamics (CFD) analysis based on a single-domain structured moving mesh obtained by novel grid generation procedure. The real-time mass flow rate, rotor torque, pressure distribution, velocity field were obtained from 3D CFD calculations. The performance curves under variable rotation speed and variable discharge pressure were produced. The CFD model was validated by comparing the simulation results of the A-type pump with the experimental data. In order to get the performance characteristics of D-type profile, two rotors with D-type profile were designed. The first has the same displacement volume as A-type and the second has the same lead and rotor length as A-type but different displacement volume. The comparison of results obtained with two rotor profiles gave an insight in the advantages and disadvantages of each of two rotor profiles analysed.

Keywords: Twin-screw pump; Rotor profile; Performance; CFD; Moving mesh

Nomenclature			
a	centre distance of two rotors	f	function of enveloping
R_1	tip radius of the male rotor	1	male rotor
R_2	tip radius of the female rotor	2	female rotor
S_m	cross section area of the male rotor	ab	epicycloid in A-type rotor profile
S_f	cross section area of the female rotor	bc	involute in A-type rotor profile
S_{acbd}	the shaded area *acbd*	cd	hypocycloid in A-type rotor profile
t	time-step or variable	ϕ	angle of rotation
$DPTS$	the degree of rotation per time step	u	velocity
RPM	rotation speed of male rotor	Σ	rotor profile
i_{12}	transmission ratio	R_t	tip circle radius
θ	centre angle of an arc	R_r	root circle radius
τ	position angle of a curve	r_1	pitch circle radius of male rotor
ω	angular velocity of rotor	r_2	pitch circle radius of female rotor
α	the angle of straight line in D-type	ρ	density

Ω	control volume	Γ	diffusion coefficient
$\boldsymbol{n}$	cell face normal vector	$\boldsymbol{v}$	fluid velocity
S	cell surface	$\boldsymbol{v_b}$	surface velocity
$q_{\phi s}$	flux source	$q_{\phi v}$	volume source

1. Introduction

Twin screw pumps are positive displacement machines widely used in petrochemical, shipping, energy and food industries due to their reliability and excellent performance in single phase or multiphase operation. Typical arrangement of a twin screw multiphase pump is given in Figure 1, showing rotors synchronised by timing gears and enclosed in the casing. Increasing demands for high-performance screw pumps require continuous improvements of pump designs to achieve better performance with higher reliability. Among the factors that influence the performance of screw pumps, rotor profile plays a vital role. Different rotor profile brings different performance characteristics. Recent developments in manufacturing technologies allow accurate production of rotors with complex rotor profiles.

The rotor profiles of multiphase screw pumps are usually different than the rotor profiles of screw compressors even though these machines are similar in configuration. Firstly, the working fluid for pumps is either liquid or multiphase fluid consisting mainly of liquid and relatively small amount of gas, contrary to screw compressors. Therefore, the working process in a pump usually does not include internal compression of gas and consequently screw pumps operate at almost constant temperature. As a consequence, inlet and outlet ports are different. The inlet and outlet ports in screw pumps are usually designed as an open type for easier suction and discharge.
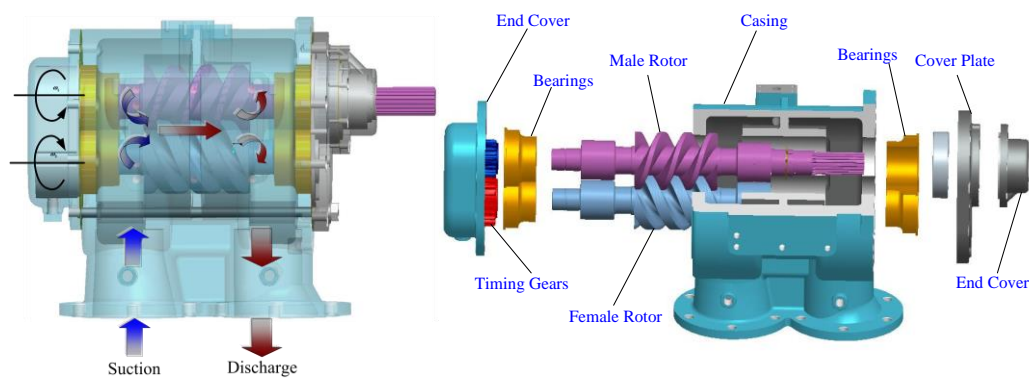

Figure 1 Structure and components of twin-screw pump

Rotor profiles for screw pumps are mainly composed of arcs which could be involute, cycloid or circular, as shown in four different types of screw pump profiles in Figure 2. Optimal rotor profiles will be different for different working conditions. The main constraints which need to be considered during the designing process of a screw pump profile are:

- The rotor profile should satisfy meshing conditions during the working process with conjugate motion and without undercutting[8][15];
- The rotor profile should have good sealing property with as small as possible blowhole,

short and continuous contact line;

- The rotor profile should have large flow area to ensure as large as possible mass flow rate;

- The carryover of the designed profile which is the area between two rotors in the default position (shown in Figure 2) should be as small as possible.

- The rotor profiles should be relatively easy to produce with as low as possible manufacturing costs.
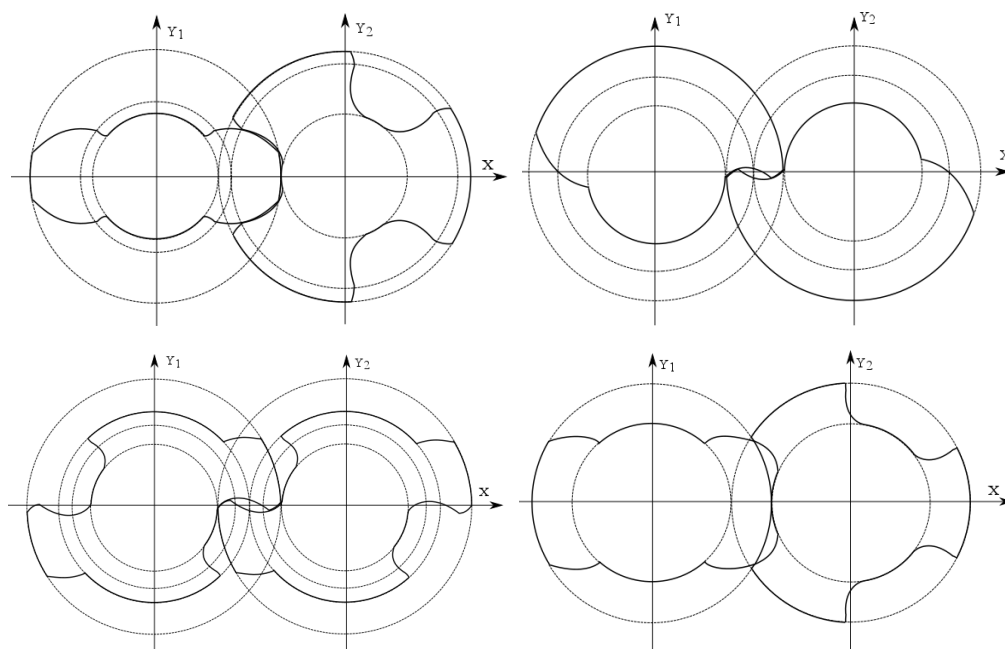

Figure 2 Four typical rotor profiles for multiphase screw pumps: A-type, B-type, C-type and D-type

Research work on rotor profile design and performance calculation of multiphase twin-screw pumps was reported in many previous studies. The number of literature resources is large and therefore just the most relevant are be listed below.

O.A. Пыж etc. [1] introduced the generation and analysis of four typical rotor profiles for marine screw pumps, which are mainly composed of involute and cycloid curves. They mentioned that even though the involute-cycloid screw pumps may not be as volumetrically efficient as cycloid screw pumps, they have higher reliability during operation. F. Li and S. Nie et al. [2][3] discussed systematically the structure, rotor profiles generation and performance calculation of different screw pump profiles and optimised some of the profiles to achieve better sealing. F. Cao, Z.W. Xing et al. [4] proposed calculation models for the back flow and pressure distribution within the multiphase twin-screw pump and also simulated the thermodynamic performance of the pump with different gas volume fractions. Q. Tang and Y.X. Zhang [5] modelled the screw pump by use of CFD static mesh and proposed improvements to a leakage model for twin-screw pump. In addition they optimised some rotor profiles. Litvin et al. [6][7][8] proposed the rotor profile generation method of roots blower and cycloidal pump based on gearing theory. N. Stosic et al. [9] applied the rack generation profiling of screw compressor to vacuum and multiphase screw pumps. They reviewed several typical rotor profiles for screw pumps using thermodynamic chamber model. C.F. Hiseh, Z.H. Fong et al. [10] investigated the

opportunities for producing rotor profiles of claw-type screw vacuum pump by theory of gearing and undercutting, and analysed the gas sealing property claimed in some patents on screw rotor rotor profiles. Jing Wei [11] discussed the rotor profile design of twin-screw kneader and simulated the flow field based on CFD by use of static grid. K. Rabiger [12] proposed a model for screw pump and carried out the numerical and experimental analysis of the performance of the pump under very high gas volume fractions (90%-99%). He also conducted an experiment to visualize the leakage flow in radial clearances [13].

For improvements in the design of screw pumps, full understanding of process within the pump is required. To date, most of the models for their performance analysis are based on the thermodynamic chamber mathematical models which neglect kinetic energy and simplify the analysis of the main and leakage flows. Chamber models can predict integral performance of screw pumps relatively accurately but are not capable of analysing flows through ports and taking into account 3D effects within the working domains.

Similarly, CFD models which use static mesh of moving flow domains to evaluate leakages are useful but do not account for dynamic effects and performance. Due to the limitation of CFD simulation using static mesh, some important parameters cannot be obtained, such as the mass flow rate, rotor torque and pressure fluctuation.

Breakthrough in using CFD for analysis of positive displacement screw machines was made by Kovacevic [14] who generated structured moving mesh for screw compressor rotor based on a rack generation method proposed by Stosic [15]. This pioneering work in grid generation for screw machines allowed for the CFD simulation and performance prediction of screw compressors. This method provided a powerful basis for research of screw pumps.

In this paper, the unique grid generation software SCORG is used for grid generation of a structured moving mesh around screw pump rotors. The mesh of stationary domains such as ports and pipes is generated by use of a commercial grid generator built into the CCM (Computational Continuum Mechanics) solver STAR-CCM+. Handling of the mesh generated by SCORG in STAR-CCM+ solver is managed by use of the UDF made specially for handling conformal rotor mesh and it will be described later in the paper.

The objective of this paper is to analyse difference in performance of 2-3 lobe combination of a twin screw pumps with different rotor profiles by use of 3D CFD.

2. Rotor profile generation for twin screw pumps
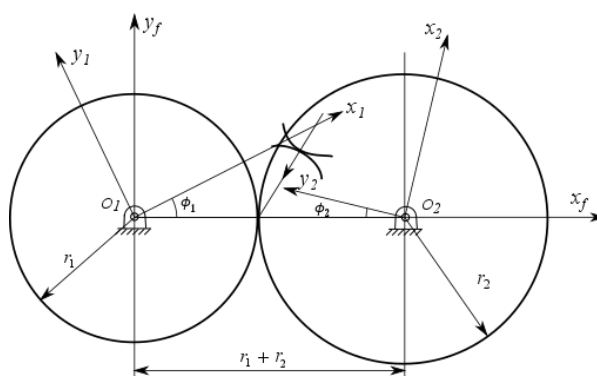
2.1 Meshing equation

Figure 3 Coordinate systems for derivation of conjugate rotor profiles

A screw pump rotor profile should satisfy the meshing principle by which the profiles of two rotors need to be conjugate without undercutting each other. Figure 3 shows the coordinate systems for derivation of conjugate rotor profiles.

The envelope equation of conjugate meshing of $\sum_2$ can be written as follows [6][8]

$$f(u, \theta, \phi) = \left(\frac{\partial \mathbf{r}_2}{\partial u} \times \frac{\partial \mathbf{r}_2}{\partial \theta} \right) \cdot \frac{\partial \mathbf{r}_2}{\partial \phi} = 0$$

Whereby, the curvilinear coordinates (u, θ) of $\sum_1$ is with the generalized parameter of motion, ϕ.

According to the theory of gearing [8], the conditions of rotor not undercutting can be written as follows

$$\begin{vmatrix} \frac{dx_1}{d\theta_1} & -\boldsymbol{v}_{x_1}^{(12)} \\ \frac{\partial f}{\partial \theta_1} & -\frac{\partial f}{\partial \phi_1} \frac{d\phi_1}{dt} \end{vmatrix} = 0; \quad \begin{vmatrix} \frac{dy_1}{d\theta_1} & -\boldsymbol{v}_{y_1}^{(12)} \\ \frac{\partial f}{\partial \theta_1} & -\frac{\partial f}{\partial \phi_1} \frac{d\phi_1}{dt} \end{vmatrix} = 0, \quad \frac{dx_1/d\theta_1}{dy_1/d\theta_1} = \frac{v_{x_1}^{(12)}}{v_{y_1}^{(12)}}$$

2.2 Involute-cycloid Rotor Profile - A-type

The rotor profile in this twin-screw pump (see Figure 4) is composed of epicycloid, hypocycloid and involute curves. The involute-cycloid rotor profile called A-type Profile is generated by modification of a cycloid rotor profile. The aim of this modification is to increase the flow area and consequently improve performance.
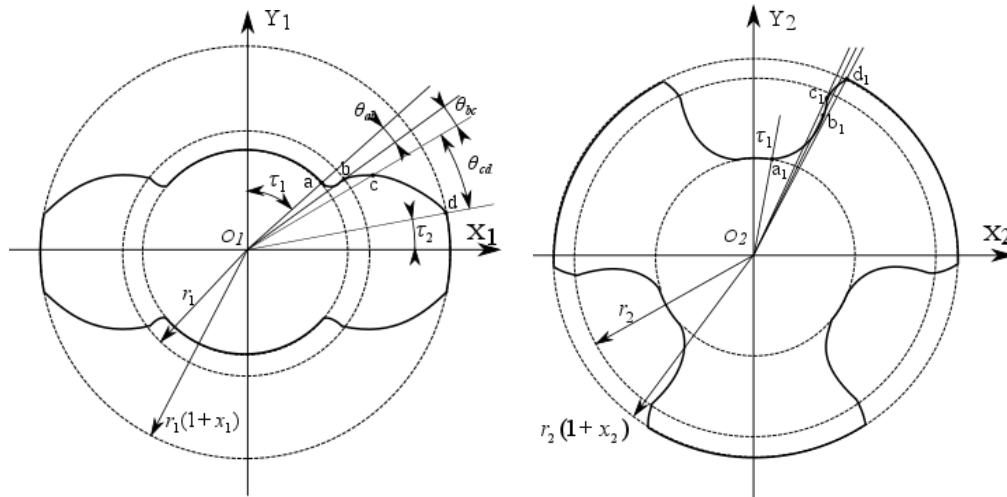

Figure 4 Generation of A-type rotor profile

Epicycloid **ab**: $t_i \leq t \leq t_j$

$$\begin{bmatrix} x_{ab} \\ y_{ab} \\ 1 \end{bmatrix} = \begin{bmatrix} -\sin(t - \tau_1) & \sin(5/3\, t - \tau_1) & 0 \\ \cos(t - \tau_1) & -\cos(5/3\, t - \tau_1) & 0 \\ 0 & 0 & 1 \end{bmatrix} \begin{bmatrix} a \\ b \\ 1 \end{bmatrix}$$

Involute **bc**: $t_i \leq t \leq t_j$

$$\begin{bmatrix} x_{bc} \\ y_{bc} \\ 1 \end{bmatrix} = \begin{bmatrix} \sin(t+\tau_1+\theta) & t\sin(t+\tau_1+\theta) & 0 \\ \cos(t+\tau_1+\theta) & -t\cos(t+\tau_1+\theta) & 0 \\ 0 & 0 & 1 \end{bmatrix} \begin{bmatrix} r \\ r \\ 1 \end{bmatrix}$$

Whereby, $\theta = \theta_{ab}$

Hypocycloid $\boldsymbol{cd}$: $t_i \le t \le t_j$

$$\begin{bmatrix} x_{cd} \\ y_{cd} \\ 1 \end{bmatrix} = \begin{bmatrix} \sin(t+\tau_1+\theta) & -\sin(5/3\,t+\tau_1+\theta) & 0 \\ \cos(t+\tau_1+\theta) & -\cos(5/3\,t+\tau_1+\theta) & 0 \\ 0 & 0 & 1 \end{bmatrix} \begin{bmatrix} a \\ b \\ 1 \end{bmatrix}$$

Whereby, $\theta = \theta_{ab} + \theta_{bc} - \theta_{2c}$,

Epicycloid $\boldsymbol{a_1b_1}$: $t_i \le t \le t_j$

$$\begin{bmatrix} x_{a_1b_1} \\ y_{a_1b_1} \\ 1 \end{bmatrix} = \begin{bmatrix} -\sin(t-\tau_2) & -\sin(5/2\,t-\tau_2) & 0 \\ \cos(t-\tau_2) & -\cos(5/2\,t-\tau_2) & 0 \\ 0 & 0 & 1 \end{bmatrix} \begin{bmatrix} a \\ b \\ 1 \end{bmatrix}$$

Involute $\boldsymbol{b_1c_1}$: $t_i \le t \le t_j$

$$\begin{bmatrix} x_{b_1c_1} \\ y_{b_1c_1} \\ 1 \end{bmatrix} = \begin{bmatrix} \sin(t+\tau_2+\theta) & -t\sin(t+\tau_2+\theta) & 0 \\ \cos(t+\tau_2+\theta) & t\cos(t+\tau_2+\theta) & 0 \\ 0 & 0 & 1 \end{bmatrix} \begin{bmatrix} r \\ r \\ 1 \end{bmatrix}$$

Whereby, $\theta = \theta_{a_1b_1}$

Hypocycloid $\boldsymbol{c_1d_1}$: $t_i \le t \le t_j$

$$\begin{bmatrix} x_{c_1d_1} \\ y_{c_1d_1} \\ 1 \end{bmatrix} = \begin{bmatrix} \sin(t+\tau_2+\theta) & -\sin(5/2\,t+\tau_2+\theta) & 0 \\ \cos(t+\tau_2+\theta) & -\cos(5/2\,t+\tau_2+\theta) & 0 \\ 0 & 0 & 1 \end{bmatrix} \begin{bmatrix} a \\ b \\ 1 \end{bmatrix}$$

Whereby, $\theta = \theta_{a_1b_1} + \theta_{b_1c_1} - \theta_{c_1d_1}$

2.3 Cycloid Rotor Profile - D-type
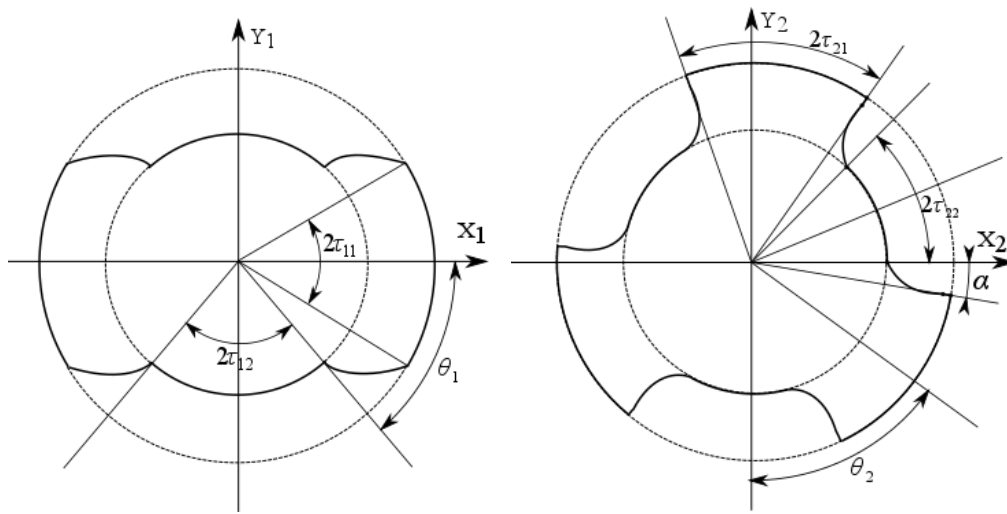

Figure 5 Generation of D-type rotor profile

Figure 5 shows the generation of D-type rotor profile which is mainly composed of cycloid

6

<div align="center">arc and circle arc.</div>

Main Rotor

Cycloid Curve:

$$\begin{bmatrix} x_{11} \\ y_{11} \\ 1 \end{bmatrix} = \begin{bmatrix} \cos t & -\cos(1 + i_{21})t & 0 \\ \sin t & -\sin(1 + i_{21})t & 0 \\ 0 & 0 & 1 \end{bmatrix} \begin{bmatrix} a \\ R_t \\ 1 \end{bmatrix}$$

Female Rotor

Epicycloid:

$$\begin{bmatrix} x_{21} \\ y_{21} \\ 1 \end{bmatrix} = \begin{bmatrix} \cos t & -\cos(1 + i_{12})t & 0 \\ \sin t & -\sin(1 + i_{12})t & 0 \\ 0 & 0 & 1 \end{bmatrix} \begin{bmatrix} a \\ R_t \\ 1 \end{bmatrix}$$

Straight line modification:

The length of the straight line $L = 0.05 R_t$

By solving the following equation

$$x_2^2 + y_2^2 = (R_t - 0.05 R_t)^2$$

Then the coordinates of the intersection point (m, n) can be obtained.

The angle between the radial straight line and the x-axis is

$$\alpha = \arctan\left(\frac{n}{m}\right)$$

The equation of the straight line is as follows:

$$x_{22} = R_t \cos t \cos\alpha$$
$$y_{22} = R_t \cos t \sin\alpha$$

The envelope line of the straight line modification in male rotor can be expressed as

$$\begin{cases} x_{12} = a\cos t - R_t u \cos(1 + i_{21})t \\ y_{12} = a\sin t - R_t u \sin(1 + i_{21})t \\ \dfrac{\partial x_{12}}{\partial u} \cdot \dfrac{\partial y_{12}}{\partial t} - \dfrac{\partial x_{12}}{\partial t} \cdot \dfrac{\partial y_{12}}{\partial u} = 0 \end{cases}$$

Whereby, $u = f(t)$, and,

$$\begin{bmatrix} x_{12} \\ y_{12} \\ 1 \end{bmatrix} = \begin{bmatrix} \cos t & -f(t)\cos(1 + i_{21})t & 0 \\ \sin t & -f(t)\sin(1 + i_{21})t & 0 \\ 0 & 0 & 1 \end{bmatrix} \begin{bmatrix} a \\ R_t \\ 1 \end{bmatrix}$$

Then the equation of cycloid curve in male rotor is

$$\begin{bmatrix} x'_{11} \\ y'_{11} \\ 1 \end{bmatrix} = \begin{bmatrix} \cos t & -\cos(1 + i_{21})t & 0 \\ \sin t & -\sin(1 + i_{21})t & 0 \\ 0 & 0 & 1 \end{bmatrix} \begin{bmatrix} a \\ 0.95 R_t \\ 1 \end{bmatrix}$$

Where, R_t is tip circle radius, R_r is root circle radius, r_1 is pitch circle radius of male rotor and r_2 is pitch circle radius of female rotor,

Transmission ratio

$$i_{12} = \frac{n_1}{n_2} = \frac{\omega_1}{\omega_2} = \frac{r_2}{r_1},$$

center distance $a = R_t + R_r$

The tip of female rotor and the root of male rotor can also be modified by the round corner modification method.

It can be observed that D-type profile is composed of cycloid, while the A-type profile consists of three profile curves, namely epicycloid, involute and hypocycloid. This makes it more difficult to generate and manufacture.

2.4 Area Efficiency

The area efficiency is the ratio of the free flow area and the overall cross section area. Large area efficiency leads to large flow passages and large flow rate under the same diameter and lead. Area efficiency is the main reference index when designing large flow screw pumps.

For twin-screw pumps, the area efficiency can be described as follows (shown as Figure 6):

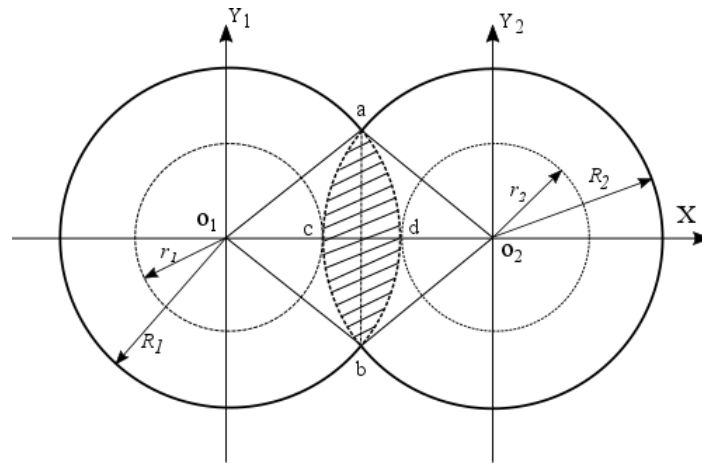$$\eta_A = 1 - \frac{S_m + S_f}{\pi R_1^2 + \pi R_2^2 - S_{abcd}} \tag{1}$$

Figure 6 Calculation of area efficiency

By using Equation (1), area efficiency of A-type and D-type rotor profiles can be calculated as:

Table 1 Area efficiency of A-type and D-type rotor profiles

	S_m (mm^2)	S_f (mm^2)	$\pi R_1^2 + \pi R_2^2 - S_{acbd}$ (mm^2)	area efficiency
A-type	7269.23	10631.61	28566.38	37.34%
D-type	10835.49	11019.14	29986.01	27.12%

Table 1 shows that the area efficiency of A-type rotor profile is approximately 1.4 times of D-type, which means theoretically the flow rate of A-type is roughly 1.4 times of D-type when all other rotor parameters are same. In order to improve the area efficiency of D-type profile, this kind of rotor profile is usually applied in the designing of three-screw pumps, which has a configuration of one male rotor and two relatively smaller female rotors.

2.5 Blowhole

<div align="center">(A-type)   (D1-type)   (D2-type)</div>
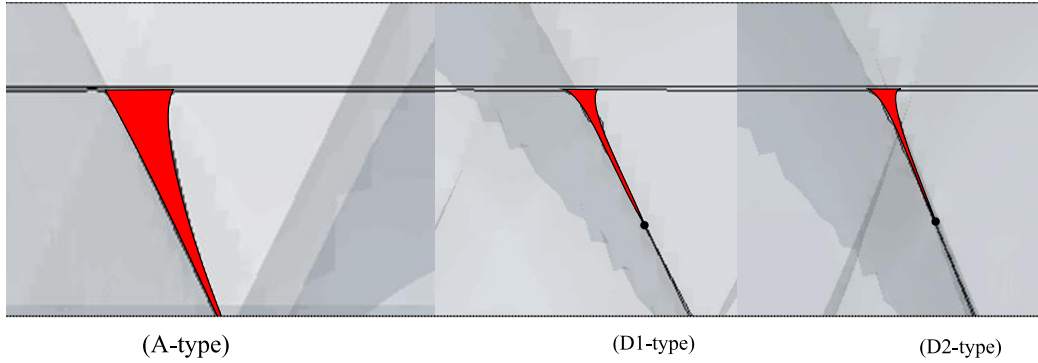
<div align="center">Figure 7 Blowhole of three kinds of rotors</div>

Figure 7 shows the blowholes of three different rotor profiles. It is obtained by inserting a plane passing the intersection line of two rotor cylinders. The A-type rotor profile results in a larger blowhole area than D-type rotors. D1 and D2 rotor profiles have the same shape of the blowhole, whereby the blowhole of D1 is slightly larger than that of D2 which is the consequence of the larger lead and helix angle of the former. From this discussion it can be concluded that leakage through blowhole area of D-type rotor profiles will be smaller than A-type rotor profiles.

3. 3 Dimensional Computational Fluid Dynamics Analysis

3.1 Mathematical Model

Positive displacement screw pumps operate on the basis of changing the size and position of the working domain which consequently causes change in the pressure of the domain which causes transports of the fluid. To calculate performance of a screw pump, quantities such as mass, momentum, energy etc. need to be obtained. Conservation of these quantities can be represented by a general transport equation for a control volume (2), [16]

$$\underbrace{\frac{\partial}{\partial t}\int_{\Omega}\rho\phi d\Omega}_{transient} + \underbrace{\int_{S}\rho\phi v.\boldsymbol{n}dS}_{convection} = \underbrace{\int_{S}\Gamma\ grad\ \phi.\boldsymbol{n}dS}_{diffusion} + \underbrace{\int_{S}q_{\phi s}dS}_{source} + \underbrace{\int_{\Omega}q_{\phi v}d\Omega}_{source} \qquad (2)$$

In order to account for the deformation of the working domain, the conservation equation (2) needs to account for the velocity of the domain boundary. This could be done by replacing the velocity in the convective term with the relative velocity $(\boldsymbol{v} - \boldsymbol{v_b})$, where $\boldsymbol{v_b}$ is the velocity vector at the cell face. In such case, the general conservation equation can be written as,

$$\underbrace{\frac{d}{dt}\int_{\Omega}\rho\phi d\Omega}_{transient} + \underbrace{\int_{S}\rho\phi(\boldsymbol{v} - \boldsymbol{v_b}).\boldsymbol{n}dS}_{convection} = \underbrace{\int_{S}\Gamma\ grad\ \phi.\boldsymbol{n}dS}_{diffusion} + \underbrace{\int_{S}q_{\phi s}dS}_{source} + \underbrace{\int_{\Omega}q_{\phi v}d\Omega}_{source} \qquad (3)$$

The grid velocity $\boldsymbol{v_b}$ and the grid motion are independent of the fluid motion. However, when the grid velocities are calculated explicitly and used to calculate the convective fluxes, the conservation of mass and other conserved quantities may not necessarily be preserved. To ensure full conservation of these equations, the space conservation law given by (4) needs to

9

be satisfied.

$$\frac{d}{dt}\int_{\Omega}d\Omega - \int_{S}\boldsymbol{v_b}.\boldsymbol{n}dS = 0 \qquad (4)$$

Space conservation can be regarded as mass conservation with zero fluid velocity. The unsteady term in governing equations involving integration over a control volume Ω, which is now changing with time, need to be treated consistently with the space conservation of a deforming and/or moving grid.
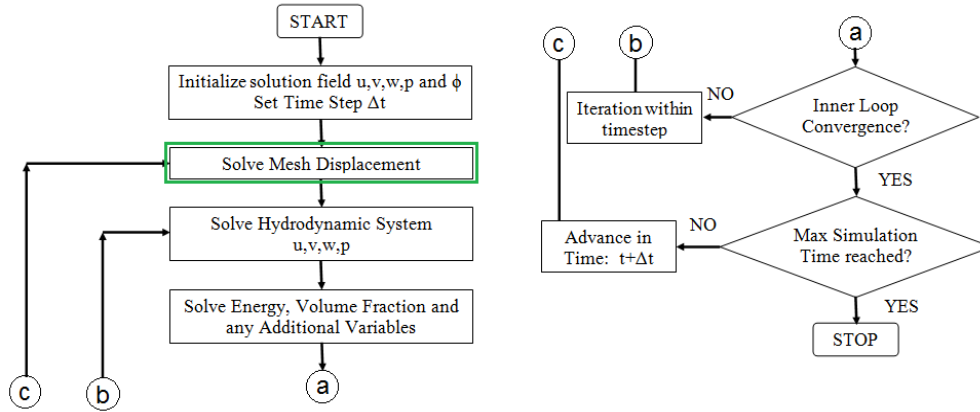

Figure 8 Flow chart of solution process with deforming domains

Governing equations required for the solution form a closely coupled, time dependent set of partial differential equations (PDE's) and often can be solved by use of a Finite Volume Method (FVM).

Figure 8 represents a flow chart of the solution process for a FVM with deforming domains. The highlighted step for resolving the mesh displacement is crucial for ensuring space conservation which requires the grid velocities and changes in CV volumes to be known at each new time step.

Providing that the numerical mesh used for transient calculation of a screw pump has a structured topology with the constant number of computational cells for any rotor position, then the movement of vertices which define the mesh can be used for calculation of wall velocity $\boldsymbol{v_b}$ ensuring that the space conservation and the entire solution are fully conservative.

However, if the numerical mesh does not keep the same topology throughout transient calculation, it is much more difficult to fulfil the conservativeness requirements. Demirdzic et al. [17] showed that the error in mass conservation due to non-conformance of space conservation is proportional to the time step size for constant grid velocities and is not influenced by the gird refinement size. This has been investigated by Rane et al. [18] to test if the user defined node displacement for structured mesh can be replaced by so called key-frame re-meshing which is the most common method normally used for deforming unstructured meshes. It was found that many limitations to key-frame re-meshing exist which make it unsuitable for analysis of screw machines. Namely, it requires time consuming pre-processing, has limited applicability to complex meshes and leads to inaccuracies in conservation of calculated variables.

Grid generation is a process of discretising a working domain of the screw pump in control volumes for which a solution of local fluid properties is to be found. It may be numerical,
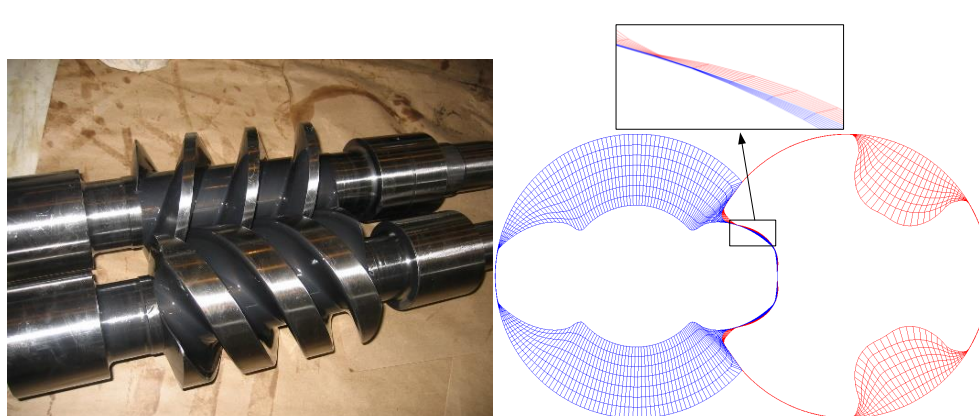
10

analytical or variational [19]. The results obtained in this research work used grids generated by analytical grid generation. Applying the principles of analytical grid generation through transfinite interpolation with adaptive meshing, the authors have derived a general, fast and reliable algorithm for automatic numerical mapping of arbitrary twin screw machine geometry built into an in-house grid generation code SCORG [20].

3.2 Moving Grid Generation

Three rotor profiles are compared in this paper, namely A-type, D1-type and D2-type. These all are with the same rotor diameter 140*mm* and equal inter-lobe and radial clearance of 0.12*mm*. The D1-type rotor is designed to have same displacement as A-type at 2100rpm; D2-type rotor is designed to have the same lead and rotor length as A-type. The design data is shown in Table 2.

Table 2 Geometric parameters of three kinds of rotors

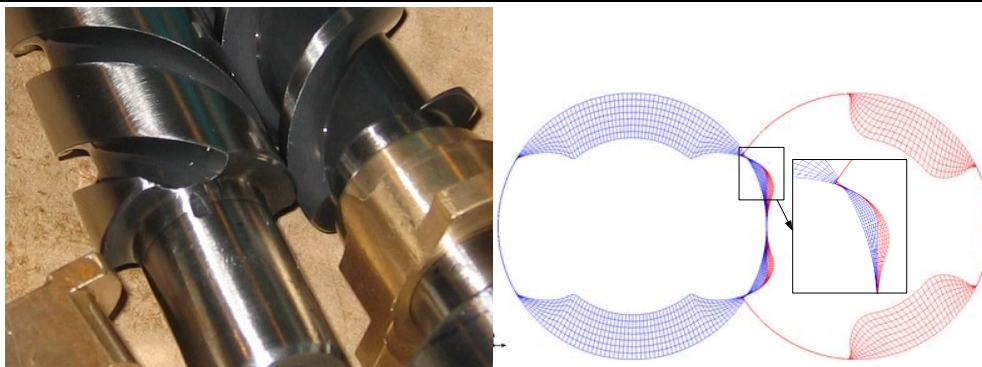| Design Data	A-type		D1-type		D2-type		Unit
	Main Rotor	Gate Rotor	Main Rotor	Gate Rotor	Main Rotor	Gate Rotor	
Axis Distance	105.025	105.025	117.6	117.6	117.6	117.6	*mm*
Outer Diameter	141	141	141	141	141	141	*mm*
Pitch Diameter	80.02	126.03	94.08	141.12	94.08	141.12	*mm*
Inner Diameter	70	70	94	94	94	94	*mm*
Rotor Length	200.004	200.004	328.996	328.996	199.995	199.995	*mm*
Wrap Angle	590.147	393.431	755.903	503.935	590.147	393.431	*Degree*
Lead	122.006	183.009	156.685	235.027	122	183	*mm*
Lead Angle	24.807	24.807	27.929	27.929	22.43	22.43	*Degree*
Helix Angle	65.193	65193	62.071	62.071	67.57	67.57	*Degree*
Depth of Groove	35.5	35.5	23.5	23.5	23.5	23.5	*mm*
Theoretical Capacity	1.302×10^{-3}		1.274×10^{-3}		0.992×10^{-3}		m^3
radial clearance	0.12		0.12		0.12		*mm*
inter-lobe clearance	0.12		0.12		0.12		*mm*

Figure 9 A-type rotors (top) and D-type rotors (bottom) with the grid distribution in a cross section

Figure 10 Surface grid of A-type, D1-type and D2-type rotors (from left to right)

Numerical grids of the working domains for the three different rotor profiles generated by SCORG are shown in Figure 9 and Figure 10. Polyhedral mesh of the inlet port and outlet port is generated using STAR-CCM+ grid generator as shown in Figure 11. The size of the numerical mesh for all three cases is shown as Table 3. The grid independence for this calculation model has already been investigated in another publication [21].
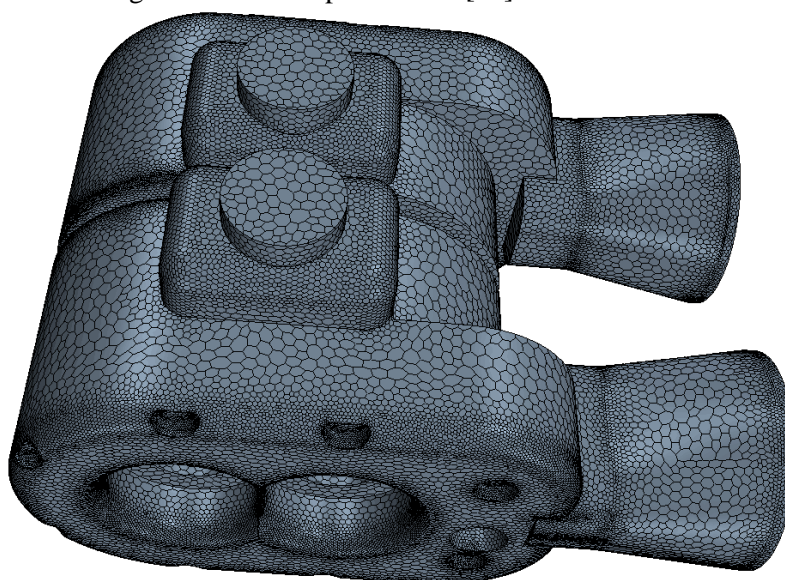

Figure 11 Polyhedral mesh of suction and discharge ports

Table 3 Number of cells used in calculation

	Suction Port	Rotor domain	Discharge Port	In Total
A-type	146842	775180	146842	1068864
D1-type	146842	993496	146842	1287180
D2-type	146842	775180	146842	1068864

3.3 Boundary Conditions and Numerical Scheme

The Star-CCM+ pressure-based solver is used for calculation of the screw pump performance. In order to solve the pressure-velocity coupling, the implicit unsteady segregated flow scheme has been applied. The second-order upwind discretization scheme is applied. Gauss-Seidel node is used for the relaxation scheme which provides good convergence by iteratively correcting (relaxing) the equations during multigrid cycling.

The main rotor rotates 2.4° per time step. The mesh is updated before commencing solution for each time step. The time-step is defined as:

$$t = \frac{DPTS}{6 \cdot RPM}$$

Where, *DPTS* is the degree of rotation per time step, *RPM* is the rotation speed of male rotor. Large time-steps may cause the solution to diverge. Time step is inversely proportional to the rotational speed, which means that the mesh needs to be changed for different speed in order to keep the ratio of time and spatial step constant. However, it's not always essential to keep the ratio constant but it is limited by Courant stability condition, as described by Kovacevic [14] and therefore the mesh was kept constant for all cases while Courant stability condition was always fulfilled.

The k-epsilon turbulence model was adopted for analysis. Stagnation inlet and pressure outlet are used respectively for the inlet and outlet boundaries. The relative pressure in the inlet port is 0 Pa. The initial pressure and initial velocity are set to 0 Pa and 0 m/s respectively. The turbulence intensity is set to 1% and the turbulence viscosity ratio is 10. The working fluid is CD40 lubricating oil. The density is 889 kg/m^3 and the dynamic viscosity is 5.25×10^{-2} Pa-S. The temperature of oil is 50 to 70°C.

4.   Results and Discussions

The CFD calculation with the A-type rotors has been validated by experiment in the prior publication by the authors [21], in order to confirm the accuracy and applicability of this numerical method for performance prediction of screw pumps.

4.1 Mass Flow Rate

Figure 12 indicates the mass flow rate of A, D1 and D2 profiles under different rotation angle and the same discharge pressure. The mass flow rate of the pump with D2-rotors is lower that other two cases. Two fluctuation periods during one full rotation of the male rotor could be observed, which is the consequence of lobe combination, in this case 2-3. The screw pump with A-type rotors brings larger oscillation than D1 and D2. The fluctuation range of A-type rotors is about 2.7%, however the fluctuation range of D1 and D2 are less than 0.9%. The fluctuation range of D1 rotors is even smaller than D2.
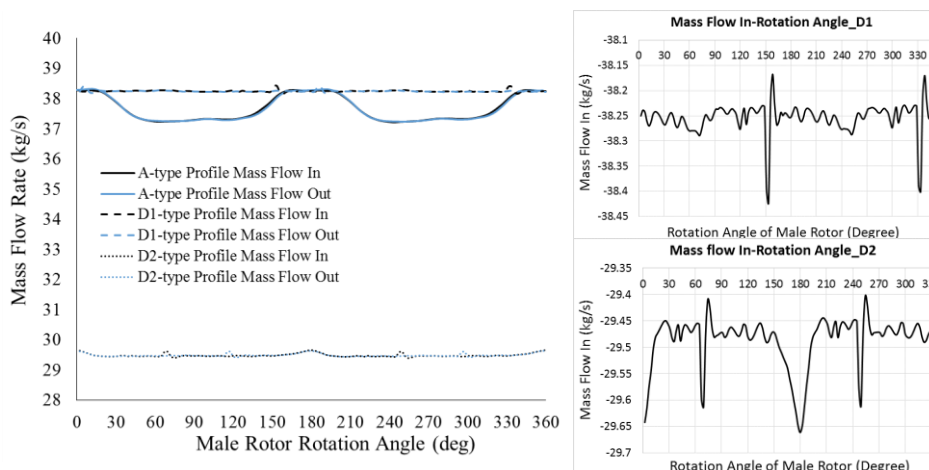
Figure 12 Mass flow rate under different rotation angle
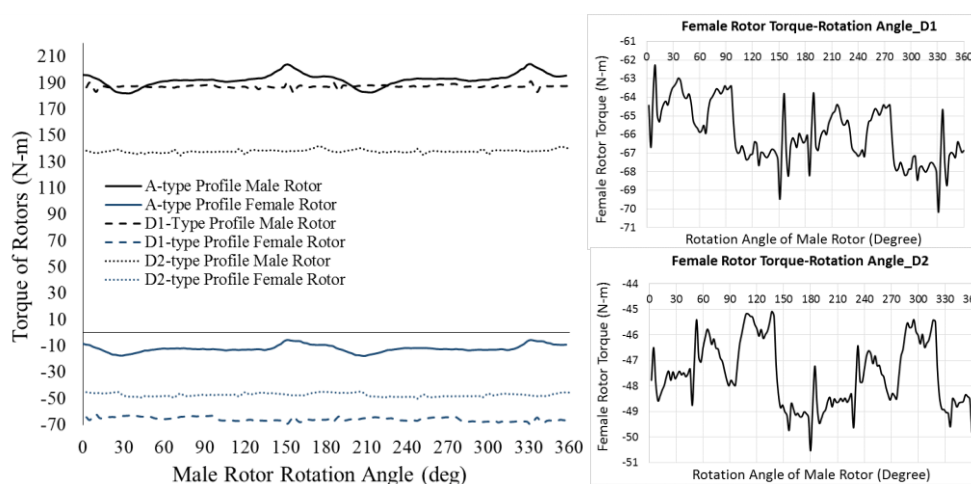
4.2 Rotor Torque

Figure 13 Rotor torque under different rotation Angle

Figure 13 shows the rotor torque of screw pump with A, D1 and D2 profiles under the same discharge pressure. Similarly to the mass flow rate, two fluctuation periods could be observed during one full rotation of the male rotor. A-type profile has higher amplitude of fluctuation of torque than D1 and D2. Figure 13 shows that the male rotor torque is much larger than the female rotor torque. The torque on the female rotor of A-type pump shows low value and low oscillations while the male rotor has large torque of approximately 190 Nm, D1-type male rotor has similar torque value but the female rotor has increased torque value, mainly due to the differences in the centre distance and rotor profile shape.
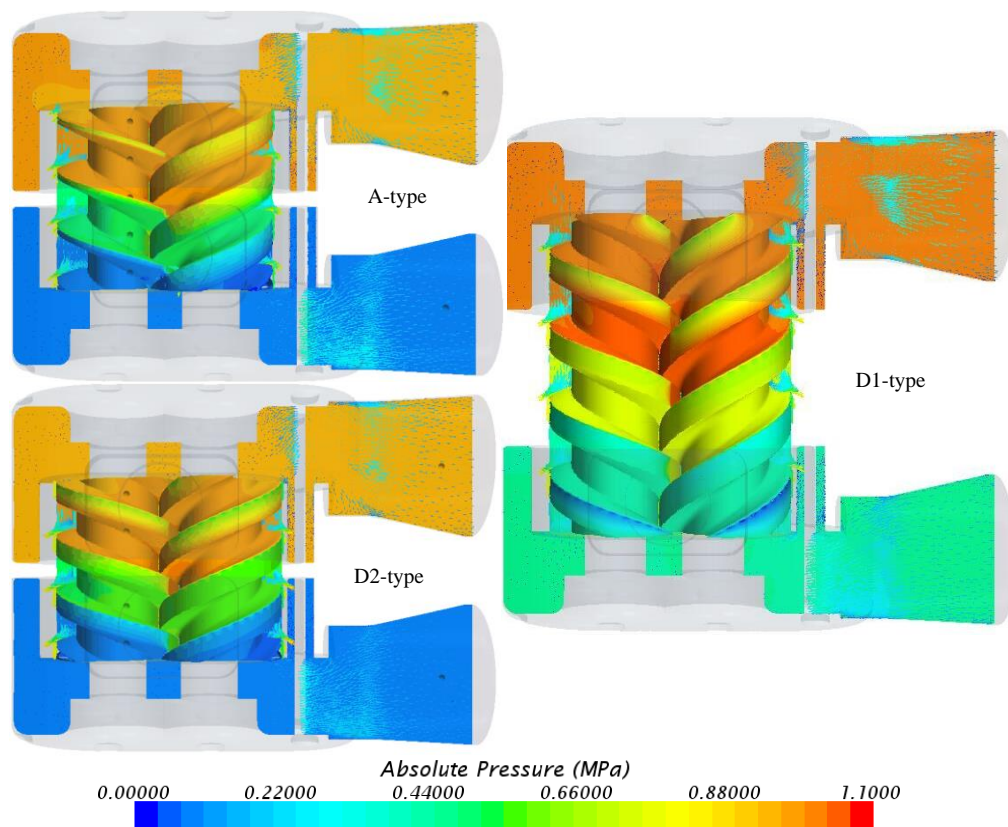
4.3 Pressure Distribution

Figure 14 Pressure distribution of three different pump designs

Figure 14 shows the pressure distribution of A, D1 and D2 pumps.

4.4 Integral Performance

Figure 15(up) shows the mass flow rate of all three pumps with the variation of rotation speed and constant discharge pressure 0.85MPa. By comparing D1 and D2, it can be found that they have the same leakage rate, which results in that the D1 has higher volumetric efficiency than D2 (shown as Figure 16). This is mainly because of the different size of the machine but also is affected by the rotor profile and different lead which in case of D1 brings higher volumetric efficiency. The A-type rotors have higher leakage rate than D1 and D2. The D-type machine has higher volumetric efficiency than A-type (Figure 16). The difference becomes smaller with the increase of rotation speed.

Figure 15(down) shows the mass flow rate at different discharge pressure and constant rotation speed of 2100rpm. Pumps with D1 with D2 profiles have nearly same leakage rate in the evaluated range of discharge pressures even though they are designed to have different lead and helix angle. However, the pump with A-type rotors have higher leakage rate than D-type, it can be easily observed under the same working condition, A-type brings larger leakage rate with the increase of discharge pressure.

Figure 16(right) shows the volumetric efficiency at different discharge pressure and constant rotation speed of 2100rpm. It can be seen that D1 has the highest volumetric efficiency among these three kind designs, then is the D2, the last is A-type. The difference becomes larger with

15
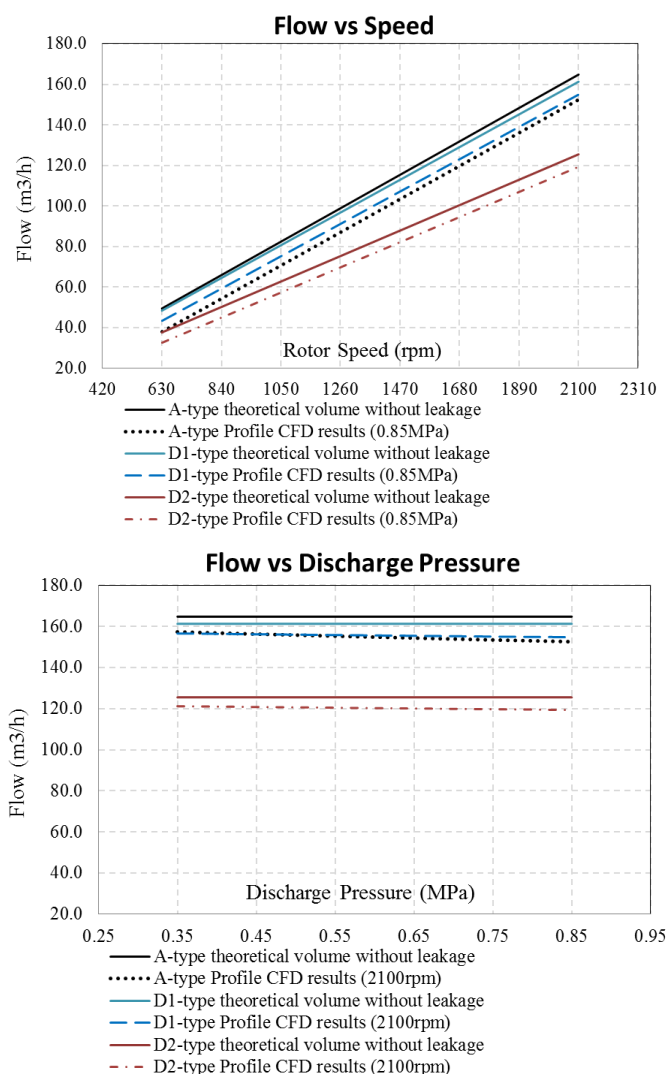
the increase of discharge pressure.

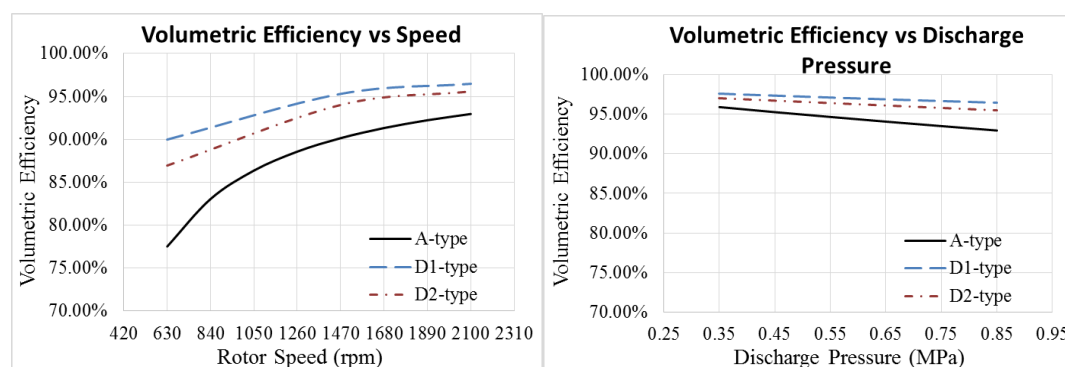Figure 15 Mass flow rate: (up) variable rotational speed; (down) variable discharge pressure

Figure 16 Volumetric Efficiency: (left) variable rotational speed; (right) variable discharge pressure
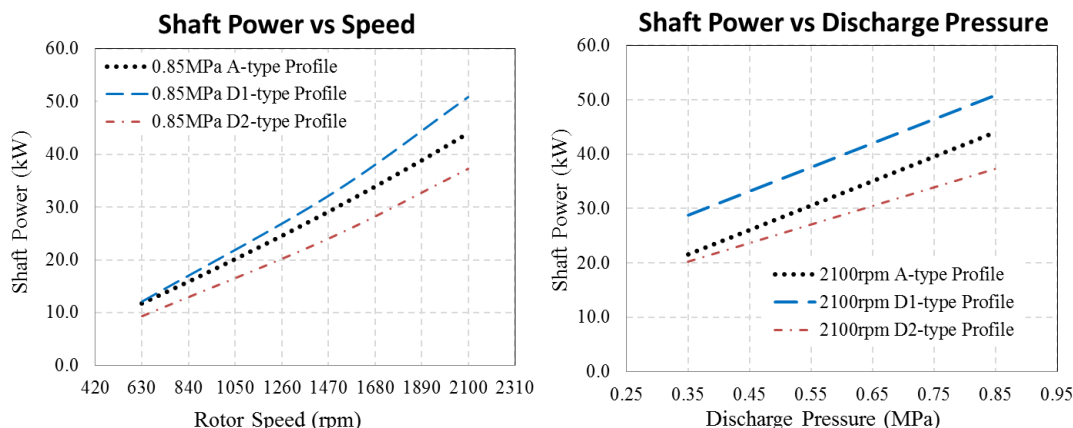
Figure 17 Shaft power: (left) variable rotational speed; (right) variable discharge pressure

Shaft power for all three pumps within the range of rotational speeds and constant discharge pressure of 0.85MPa is shown in Figure 17(left). Shaft power of the D1 pump increases with higher gradient than the shaft power of A-type pump. The shaft power at 630rpm is same for both profiles while at 2100 rpm power of D1-type pump is more than 15% higher although the flow rates are very similar. By comparing A-type and D2-type pumps, it can be observed that A-type pump has approximately 30% larger flow rate than the D2 and 15-30% higher shaft power depending on the speed. The power difference between the two stays the same while the ratio significantly decreases with the increase in speed. It is worth mentioning that both A and D2 pumps have the same lead and rotor length.

Figure 17(right) shows the shaft power as a function of discharge pressure and with constant rotation speed 2100rpm. The shaft power for A and D1 pumps follows the same trend with the increase of the discharge pressure. A-type pump has lower absolute value. The shaft power of A and D2 pumps are similar at the low discharge pressure but the difference increases with the increase in the discharge pressure. The shaft power of A-type pump is larger than that of D2-type pump. This is an indication of lower volumetric and adiabatic efficiencies of A-type pump.

5. Conclusions

A-type - involute-cycloid and D-type - cycloid based rotor profiles have been generated and analysed in this paper. In order to compare the characteristics of these two different rotor profiles, full 3D CFD simulation of three designed twin-screw pumps has been carried out using structured moving numerical mesh. Pumps A and D1 have similar theoretical displacement while pumps A and D2 have the same length, helix angle and rotor diameters and different theoretical displacements due to much shallower rotor groove of the D2 rotors.

(1) A-type rotor profile has larger area efficiency than D-type but also larger blowhole area than the D-type.
(2) For 2-3 type twin-screw pump, when increasing the area efficiency of cross section by introducing involute-cycloid profiles, the depth of the rotor groove will increase, which will bring larger the mass flow rate while lead to larger the mass flow pulsation at the same time.
(3) Even if the pump is scaled up to achieve the same flow rate, the pulsation in the D2

17

type pump will decrease compared to A-type and allow more stable operation.

(4) Rotor pumps with A-type and D-type rotor profile of the same length, rotor diameter and helix angle will have different theoretical volume and mass flow. D-type rotors have lower mass flow rate, larger rotor torque and larger power consumption, but at the same time it has an advantage of smaller fluctuation in mass flow rate and pressure and smaller leakage rate.

(5) The CFD results indicate that A-type rotor profile is more suitable for large-volume pumps, while D-type rotor profile is more suitable for high-pressure pumps.

References

[1] O.A. Пыж etc., Marine Screw Pump, Hefei General Machinery Research Institute (1969) (in Chinese).

[2] Futian Li, Screw Pump, ISBN 9787111297949, Beijing, China Machine Press, 2010.

[3] Shubin Nie, Futian Li, Weiling Lv, Yanhua Feng, Daquan Guo, Improvement and hermeticity analysis of B-type double screw pump curve, Mechanical and Electrical Equipment 26(5) (2009) 47-51 (in Chinese).

[4] Feng Cao, Yueyuan Peng, Ziwen Xing, and Pengcheng Shu. Thermodynamic Performance Simulation of a Twin-Screw Multiphase Pump. Proceedings of the IMechE, Part E: Journal of Process Mechanical Engineering, 2001: 157-162.

[5] Qian Tang, Yuanxun Zhang. Screw Optimization for Performance Enhancement of a Twin-Screw Pump. Proceedings of the IMechE, Part E: Journal of Process Mechanical Engineering, 2014, 228(1):73-84.

[6] Faydor L. Litvin, Pin-Hao Feng, Computerized design, generation, and simulation of meshing of rotors of screw compressor, Mechanism and Machine Theory 32 (2) (1997) 137–160.

[7] Faydor L. Litvin, Computerized design and generation of cycloidal gearings, Mechanism and Machinery Theory 31(7)1996, 891-911.

[8] Faydor L. Litvin, Theory of Gearing, NASA Reference Publication-1212, Washington DC, 1989

[9] Stosic N., Smith I.K., Kovacevic A., Vacuum and Multiphase Screw Pump Rotor Profiles and Their Calculation Models, Conference on Screw Type Machines VDI-Schraubenmachinen, Dortmund, Germany, October 2006.

[10] Chiu-Fan Hsieh, Yii-Wen Hwang, Zhang-Hua Fong, Study on the rotor profile for the screw claw-type pump, Mechanism and Machine Theory 43 (2008) 812-828.

[11] Jing Wei. Research on Rotor Profiles Design Method and Numerical Simulation for Twin-screw Kneader. [J].Journal Of Mechanical Engineering (Chinese Edition) 2013, Vol. 49(3): 63-73.

[12] Rabiger, K. Fluid Dynamic and Thermodynamic Behaviour of Multiphase Screw Pumps

Handling Gas-Liquid Mixtures with Very High Gas Volume Fractions. Ph.D. Thesis, Faculty of Advanced Technology, University of Glamorgan, 2009.

[13] Rabiger K, Maksoud T, Ward J, et al. Theoretical and experimental analysis of a multiphase screw pump, handling gas-liquid mixtures with very high gas volume fractions. Exp Therm Fluid Sci 2008; 32(8):1694–1701.

[14] Kovačević A., Stošić N., Smith I. K., 2006: Screw Compressors Three Dimensional Computational Fluid Dynamics and Solid Fluid Interaction, ISBN-10: 3-540-36302-5, Springer Berlin Heidelberg New York

[15] Stosic N., Smith I. K., Kovacevic A., 2005: Screw Compressors Mathematical Modelling and Performance Calculation, ISBN-10 3-540-24275-9, Springer Berlin Heidelberg New York

[16] Ferziger J H, Perić, M, 2002: Computational Methods for Fluid Dynamics 3rd Edition, ISBN 3-540-42074-6, Springer-Verlag Berlin Heidelberg NewYork

[17] Demirdžić I, Muzaferija S, 1995: Numerical Method for Coupled Fluid Flow, Heat Transfer and Stress Analysis Using Unstructured Moving Mesh with Cells of Arbitrary Topology, Comp. Methods Appl. Mech Eng, Vol.125 235-255

[18] Rane S., Kovačević A., Stošić N., 2015, Analytical Grid Generation for accurate representation of clearances in CFD for Screw Machines, 9th Int conf on compressors and their systems, 2015 IOP Conf. Ser.: Mater. Sci. Eng. 90

[19] Rane S, Grid Generation and CFD analysis of variable Geometry Screw Machines. PhD Thesis, City University London. 2015

[20] Sham Rane, Ahmed Kovacevic, Nikola Stosic, Madhulika Kethidi, Deforming grid generation and CFD analysis of variable geometry screw compressors[J].Computers & Fluids, 2014, 99:124–141

[21] Di Yan, Ahmed Kovacevic, Qian Tang, Sham Rane, Numerical Modelling of Twin-screw Pumps Based on Computational Fluid Dynamics[J].Proceedings of the IMechE, Part C: Journal of Mechanical Engineering Science (in review), 2016